Colloid Polym Sci 279:621–628 (2001)

ORIGINAL CONTRIBUTION

V. Castelletto
I. W. Hamley
P. Holmqvist
C. Rekatas
C. Booth
J. G. Grossmann

Small-angle X-ray scattering study of a poly(oxyphenylethylene)–poly(oxyethylene) diblock copolymer gel under shear flow

Received: 8 September 2000
Accepted: 29 November 2000

V. Castelletto · I. W. Hamley (✉)
P. Holmqvist
School of Chemistry, University of Leeds
Leeds LS2 9JT, UK

C. Rekatas · C. Booth
Department of Chemistry
University of Manchester
Manchester M13 9PL, UK

J. G. Grossmann
Synchrotron Radiation Source
Daresbury Laboratory, Daresbury
Warrington WA4 4AD, UK

Abstract The structure and flow behaviour of a micellar "cubic" phase is studied, using small-angle X-ray scattering (SAXS) and constant stress rheometry on a poly(oxyphenylethylene)–poly(oxyethylene) diblock copolymer in water. The predominant structure is a face-centred cubic (fcc) array of spherical micelles, which under shear undergoes layer sliding to give a scattering pattern from stacked hexagonal close-packed layers. A detailed analysis of the SAXS data indicates the presence of a fraction of grains with a structure distorted from a fcc phase. The additional reflections that characterize this structure can be indexed to a rhombohedral unit cell, space group $R\bar{3}m$, with the same volume as the fcc unit cell. The rhombohedral unit cell corresponds to a cubic cell that has been "stretched" along a [111] direction, and it is suggested that such a structure results from the gradient in shear velocity in the Couette cell employed. Shearing at high shear rates leads to a "smearing out" of the reflections, but upon cessation of shear under these conditions a highly oriented SAXS pattern is obtained, which confirms the persistence of rhombohedral ordering. The shear-induced changes in orientation are correlated to a plateau observed in the stress plotted against shear rate, such a plateau being a sign of inhomogeneous flow.

Key words Block copolymers · Micelles · Cubic phase · X-ray scattering · Shear

Introduction

It is now firmly established that shear can be used to align cubic phases of diblock copolymers [1–4]. In particular, aqueous solutions of diblock copolymers with a E_mP_n or E_mB_n architecture [the subscripts denote the number of repeats; $E = OCH_2CH_2$, oxyethylene; $P = OCH_2CH(CH_3)$ and $B = OCH_2CH(C_2H_5)$, oxypropylene and oxybutylene, respectively] have been used to perform shear-flow experiments on the cubic micellar phase, using small angle X-ray scattering (SAXS) [5–7].

Daniel et al. [5] performed SAXS experiments on an aqueous salt solution of $E_{55}B_8$ in the cubic phase, which showed that steady shear orients grains with face-centred cubic (fcc) symmetry in a polydomain with crystal planes adopting different orientations as a function of the shear rate. Relatively low shear rates induced a shear-flow mechanism attributed to the sliding of two-dimensional hexagonal close-packed (hcp) layers stacked perpendicular to the shear gradient direction [5, 8]. For higher shear rates, the diffraction pattern became more complex, showing a partial reorientation of the {111} planes in the direction perpendicular to the shear plane. Upon cessation of shear, melted grains recrystallized in a distinct orientation of a fcc crystal with a [110] direction parallel to the shear [5].

A similar coexistence of hcp layers oriented parallel and perpendicular to the shear plane was found for fcc grains in the cubic phase of a related block copolymer, $E_{40}B_{10}$ [6]. For this sample the shear-flow behaviour of

body-centred cubic (bcc) grains was also studied, and it was found that close-packed {110} planes align both parallel and perpendicular to the shear plane. A different orientation of bcc grains in the cubic phase was attained under steady shear for aqueous salt solutions of $E_{86}B_{10}$ where the crystal planes aligned with the [111] direction coincident with the shear direction and flow occurred in {110} and {211} planes [7].

It has become clear that the flow behaviour of block copolymers can be highly inhomogeneous. Flow-induced phase separation, or "shear banding", has been studied in detail for solutions of wormlike micelles [9]; however, recent work has shown that inhomogeneous flows can lead to shear banding in other soft materials, in particular, in spherical-micellar solutions of block copolymers [10]. Eiser et al. [10] have recently discussed the complex flow behaviour of bcc gels formed in aqueous solutions of triblock $E_{76}P_{30}E_{76}$ investigated by constant stress rheometry and SAXS with in situ steady shearing in a Couette cell. The flow in this cell was inhomogeneous owing to the large stress gradient (a decrease of 20% at the outer wall compared to the inner wall). Two successive orientation transitions were observed to occur at very different shear rates but were separated by a narrow difference in stress. The stress as a function of shear rate showed two plateaus, within each of which two distinct structural organizations coexisted in the gap of the Couette cell. The structure of the gel as a function of shear rate was elucidated by SAXS. In a parallel work, Eiser et al. [11] described the application of creep rheometry to study the deformation behaviour of a fcc phase formed in an aqueous solution of $E_{127}P_{48}E_{127}$, although in that case nonhomogeneous flows were not observed. In the present article, we present evidence for inhomogeneous flows in a fcc micellar phase formed by an S_nE_m [$S = OCH_2CH(C_6H_5)$, hydrophobic oxyphenylethylene unit] diblock copolymer in water.

In comparison to copolymers containing hydrophobic B or P units, little is known about the shear-flow behaviour of copolymers made with a hydrophobic block prepared from oxyphenylethylene styrene oxide. Here we report the effect of steady shear on the orientation of a cubic phase with fcc symmetry formed in a gel of diblock $S_{13}E_{60}$ in water.

This work complements an earlier study where micellar dimensions and association numbers corresponding to aqueous dilute solutions of $S_{13}E_{60}$ [12] were calculated from light-scattering results, leading to a hydrodynamic radius $r_h = (98 \pm 4.9)$ Å, a thermodynamic radius $r_t = (86 \pm 4.3)$ Å and a mass-average micellar association number $N_w = 102$.

Here we describe experiments where $S_{13}E_{60}$ gels were subjected to steady shear using a Couette cell with simultaneous SAXS. Micellar parameters are compared with the values previously obtained in the isotropic phase for $S_{13}E_{60}$ [12], while the shear-flow behaviour is analysed in the light of previous results obtained from shear-flow experiments on EB diblock copolymers in the cubic phase [5–7].

Experimental

Materials

The copolymer $S_{13}E_{60}$ was identical to the one used earlier [12]. As described elsewhere [12], it has a narrow molecular-weight distribution (i.e. the ratio of mass-average molar mass to number-average molar mass), $M_w/M_n = 1.03 \pm 0.01$ determined by gel permeation chromatography on the basis of poly(oxyethylene) calibrants, where $M_n = 4290\ \mathrm{gmol}^{-1}$ was determined from ^{13}C NMR spectra analysis [12]. We studied a 30 wt% solution of $S_{13}E_{60}$ in water, which was prepared by mixing appropriately weighed amounts of copolymer and water by diffusion over a period of days at low temperature (about 5 °C). Optical examination revealed that the gel formed by this sample was clear and did not reveal any birefringence, consistent with cubic symmetry.

Rheology

Step-shear experiments were conducted using a shear-stress controlled Bohlin CVO rheometer using a cone-and-plate fixture with a cone diameter of 40 mm and a cone angle of 4°. A constant force was applied to the sample and the displacement was measured and collected using a personal computer running Bohlin software. The samples were kept at (20.0 ± 0.1) °C with a water-flow-controlled element using a Bohlin Instruments KTB 30 thermostatic bath. To avoid evaporation, all the samples were protected with a thin film of silica oil. The step-shear experiments were made applying a constant shear stress for 300 s, measuring the shear rate for the following 200 s, and then increasing the shear stress to the next step and so forth.

Small-angle X-ray scattering

SAXS experiments were conducted on beamline 2.1 at the Synchrotron Radiation Source, Daresbury Laboratory, UK, which is configured with an X-ray wavelength $\lambda = 1.5$ Å. Details of this beamline and data collection electronics have been given elsewhere [13]. Experiments were performed with a 6-m camera. Scattered photons were collected on a multiwire gas-filled area detector. A scattering pattern from a specimen of wet collagen (rat-tail tendon) was used for calibration of the $\mathbf{q}$ scale ($|\mathbf{q}| = 4\pi \sin\theta/\lambda$, where the scattering angle is 2θ).

Samples were subjected to steady shear, using a Couette cell described in detail elsewhere [14]. Briefly, it comprises two concentric polycarbonate cylinders, with an inner stator (radius 25 mm) and an outer rotor, with a 0.5-mm gap for the sample. A cylindrical tube is incorporated in the inner stator, for the X-ray beam to pass through. The cell is mounted on a motorized translation stage, which allows the sample to be aligned in any beam position between the so-called radial and tangential configurations. The radial orientation corresponds to $\mathbf{q}$ parallel to $\nabla\mathbf{v}$, the velocity gradient direction, and provides the SAXS pattern in the ($\mathbf{q}_v$, $\mathbf{q}_e$) plane, where $\mathbf{e} = \nabla\mathbf{v} \times \mathbf{v}$ is the vorticity direction. The tangential configuration corresponds to $\mathbf{q}$ parallel to $\mathbf{v}$, the shear velocity direction, and gives access to the SAXS pattern in the ($\mathbf{q}_{\nabla v}$, $\mathbf{q}_e$) plane.

The temperature of the Couette cell was controlled using a water bath. Measurements were carried out at 20 and 50 °C. The Couette cell motor and water bath temperature were both controlled remotely using a personal computer in the hutch of the beamline. The accessible shear rate range is $0.05 < \dot{\gamma}/s^{-1} < 540$ for steady shear.

Results and discussion

We first identify the diffraction pattern of the sample at rest. This static description is followed by the presentation of the shear-flow behaviour displayed as a function of $\dot{\gamma}$ for 20 and 50 °C.

Static study of the $S_{13}E_{60}$/water system

The as-mounted sample at 20 °C showed a nearly spherically averaged powder diffraction pattern, consisting of three diffraction rings in the positional ratio $1:(4/3)^{1/2}:(8/3)^{1/2}$, in good agreement with a fcc lattice ($Fm\bar{3}m$ symmetry) [15]. The reduction of the two-dimensional data for this sample, obtained by integration of the SAXS pattern in a vertical rectangular slice, is shown in Fig. 1a. The peak at smaller scattering angles corresponds to a 111 reflection, while the higher-order peaks are 200 and 220 reflections. It is possible to calculate a cell parameter, $a = (258.9 \pm 4.3)$ Å, from the first-order reflection at $q^* = (0.0420 \pm 0.0007)$ Å^{-1}. The cell parameter provides a distance between nearest neighbours, $d = (183.1 \pm 3.0)$ Å, from which it is possible to calculate a micellar radius, $r_m = (91.6 \pm 1.5)$ Å, that is in good agreement with the hydrodynamic and thermodynamic radii given in the Introduction [12].

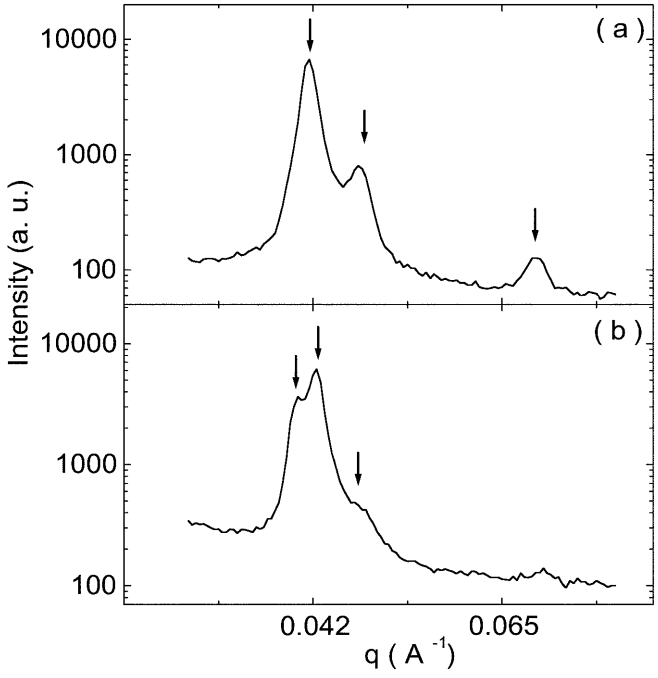

Fig. 1 Small-angle X-ray scattering (*SAXS*) intensity as a function of the scattering vector, q, obtained by integration in a vertical rectangular slice of the two-dimensional SAXS pattern measured at 20 °C for **a** the as-mounted sample and **b** the sample at rest after shear at $\dot{\gamma} = 20$ s^{-1}. The *arrows* indicate the position of the measured reflections

Shear-flow behaviour of the $S_{13}E_{60}$/water system

During shear-flow experiments, the sample was constrained to a fixed shear rate and then the shear was stopped. Data reduced to one-dimensional form obtained by integration of the SAXS pattern corresponding to the sample at rest after shear at $\dot{\gamma} = 20$ s^{-1} at 20 °C are shown in Fig. 1b. Two-dimensional SAXS patterns obtained in the ($\mathbf{q}_v$, $\mathbf{q}_e$) plane at 20 and 50 °C are compared in Fig. 2. The angular positions of the reflections obtained from the diffraction patterns shown in Fig. 2 are listed in Table 1.

SAXS patterns obtained from shear-flow experiments at 20 °C are shown in Fig. 2a and b. The main effect of the shear flow is to induce an orientation of the crystal planes. The first- and third-order rings of reflections observed for the as-mounted sample change, under shear flow, to Bragg spots arranged with a sixfold symmetry. During shear at $\dot{\gamma} = 20$ s^{-1} the SAXS pattern shows two meridional reflections, which become more pronounced when the shear is stopped, at scattering angles slightly higher than the inner set of reflections with sixfold symmetry. The contrast in Fig. 2a and b is not high enough to distinguish these meridional reflections; however, this is clarified through Fig. 1b, which shows data reduced to one-dimensional form obtained by integration of the SAXS pattern in Fig. 2b in a vertical rectangular slice, and where the first two peaks correspond, as a function of increasing q, to the reflection in the inner set with sixfold symmetry and to the meridional reflection. Four additional weak reflections are also observed in Fig. 2a and b, at 45° with respect to $\mathbf{q}_v$, at scattering angles corresponding to the second-order diffraction ring of the as-mounted sample.

As already mentioned, the Bragg spots on the external and internal rings with sixfold symmetry in Fig. 2a and b correspond to 111 and 220 reflections of a fcc structure, respectively (Table 1). Indeed, Fig. 2a and b show that these reflections are not sharp Bragg spots, but they are reinforced along diffuse scattering arcs corresponding to the orientation distribution of planes with interplanar distances equal to d_{111} and d_{220}, respectively.

The observation of 220 reflections is consistent with perfect ABCABC... fcc stacking of close-packed layers aligned parallel to the Couette cell walls, i.e. to the

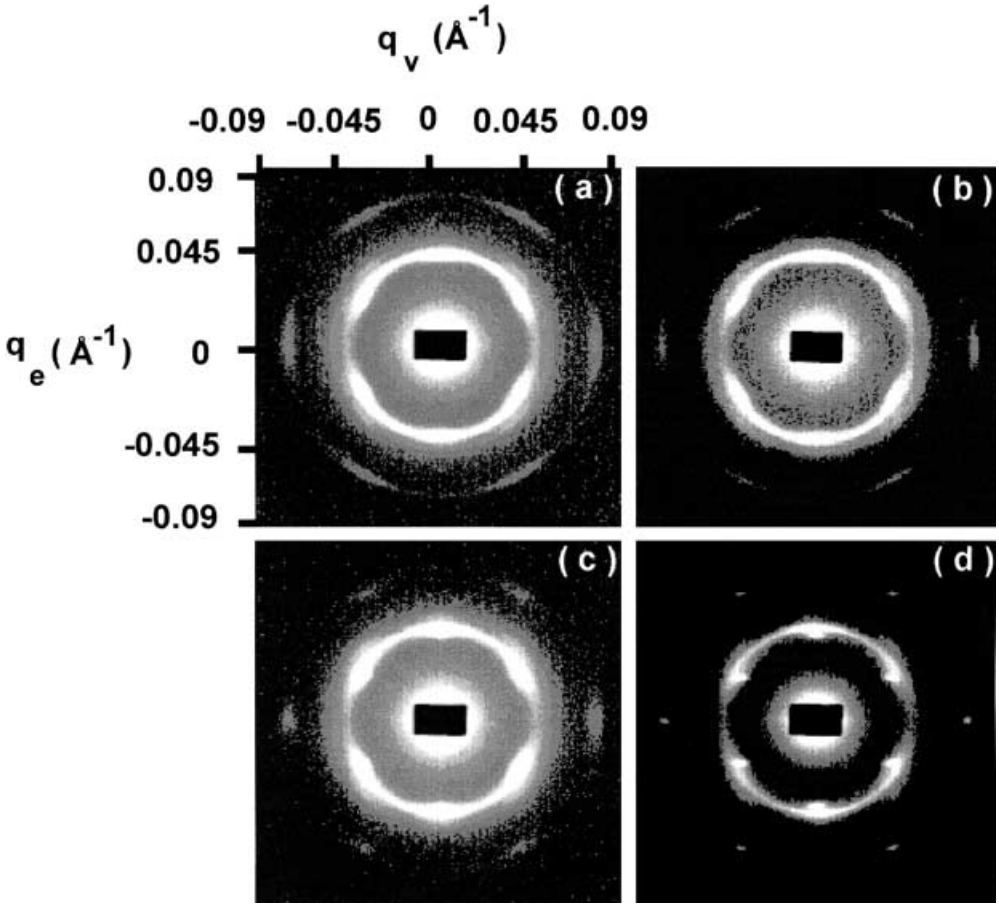

Fig. 2a–d SAXS patterns in the ($\mathbf{q_v}$, $\mathbf{q_e}$) plane. Experiments at 20 °C: **a** sample during shear at $\dot{\gamma} = 20\ s^{-1}$; **b** sample at rest after shear at $\dot{\gamma} = 20\ s^{-1}$. Experiments at 50 °C: **c** sample during shear at $\dot{\gamma} = 400\ s^{-1}$; **d** sample at rest after shear at $\dot{\gamma} = 400\ s^{-1}$

Table 1 Indexation of diffraction patterns

Temperature (°C)	$\dot{\gamma}$ (s^{-1})	q_{exp} ($Å^{-1}$)[a]	$(hkl)_{fcc}$[b]	q_{fcc} ($Å^{-1}$)[c]	ε (%)[d]	$(hkl)_r$[e]	q_r ($Å^{-1}$)[f]	ε (%)
20	20	0.0416	111	0.0420	0.9	–	–	–
		0.0429	–	–	–	$\bar{1}\bar{1}2$	0.0424	0.2
		0.0483	200	0.0486	0.6	–	–	–
		0.0698	220	0.0687	0.3	$30\bar{3}$	0.0743	6.4
20	0	0.0407	111	0.0420	3.2	–	–	–
		0.0429	–	–	–	$\bar{1}\bar{1}2$	0.0429	0
		0.0487	200	0.0485	0.4	–	–	–
		0.0707	220	0.0686	2.9	$30\bar{3}$	0.0743	5.1
50	400	0.0429	111	0.0423	0.9	–	–	–
		0.0483	200	0.0491	1.7	–	–	–
		0.0698	220	0.0694	0.6	–	–	–
50	0	0.0407	111	0.0419	2.7	–	–	–
		0.0434	–	–	–	$\bar{1}\bar{1}2$	0.0434	0
		0.0487	200	0.0482	1	–	–	–
		0.0693	220	0.0682	1.6	$30\bar{3}$	0.0752	8.5

[a] Position of the measured scattering peak
[b] Miller indices corresponding to a face-centred cubic cell
[c] Scattering vector calculated from a face-centred cubic structure
[d] Residual from the difference between experiment and calculation
[e] Miller indices corresponding to a rhombohedral cell
[f] Scattering vector calculated assuming a rhombohedral structure

($\mathbf{q_v}$, $\mathbf{q_e}$) plane. However, the simultaneous presence of 111 and 220 reflections in the diffraction patterns destroys this hypothesis. As already discussed in the literature [5, 6, 8], the presence of 111 reflections can be attributed to irregularities in the layer stacking sequence, probably due to sequences of ABAB... stacking as in a three-dimensional hcp structure.

The four weak scattering peaks observed at 45° with respect to $\mathbf{q_v}$ in Fig. 2a and b correspond to 200 reflections of a fcc lattice (Table 1) and can be ascribed to a small population of grains with {001} planes parallel to the shear plane and the {110} plane aligned parallel to $\mathbf{q_v}$, as discussed elsewhere [6, 16]. Diffuse scattering arcs, corresponding to the orientation distribution of planes with interplanar distances equal to d_{200} are superposed on 200 Bragg spots in the diffraction pattern.

A result similar to that shown in Fig. 2a and b was observed for the sample subjected to shear at $\dot{\gamma} = 200\ s^{-1}$ at 20 °C. For that particular shear rate, additional information was obtained since two-dimensional diffraction patterns recorded in the tangential configuration corresponded to a twinned structure reported previously [6]. The diffraction pattern of one of the twins had a pair of reflections ($\bar{1}\bar{1}1$ and $11\bar{1}$) on the equator and 111, $\bar{1}\bar{1}\bar{1}$ reflections at an angle $\alpha = 19°$ with respect to the meridian. Additional 002 and $00\bar{2}$ reflections were present at an angle $\beta = 35°$ with respect to the meridian. In the direct space, α and β are measured with respect to the normal to the hcp planes. The presence of equatorial 111 reflections shows that some {111} layers are stacked parallel to the ($\mathbf{q_v}$, $\mathbf{q_e}$) plane; therefore shear flow induces a mixed orientation of hcp layers parallel and perpendicular to the shear plane for $S_{13}E_{60}$, in good agreement with previous results found for fcc grains in the cubic phase of aqueous solutions of $E_{40}B_{10}$ and $E_{55}B_8$ [5, 6].

Considering the two-dimensional diffraction pattern in Fig. 2a and b, the two meridional reflections at scattering angles slightly higher than the inner set of six reflections (Fig. 1b) cannot be indexed to a fcc structure. Instead, we have considered that these peaks arise from a small fraction of grains with one of a number of other possible structures. Trial structures used were based on distorted cubic structures, motivated in part by prior work indicating the possibility of a shear-induced breaking of cubic symmetry for a fcc diblock copolymer gel [17] due to a contraction of the spacing between hcp layers. Rhombohedral and tetragonal structures break cubic symmetry. An attempt to index the meridional reflections obtained under different shear conditions listed in Table 1 to a tetragonal structure did not produce agreement as good as that found for a rhombohedral structure; therefore, the indexation in terms of a rhombohedral structure will be discussed. As indicated in Table 1, the indexation of the pair of meridional reflections just outside the inner six peaks (Fig. 1b) as $\bar{1}\bar{1}2$ reflections from a rhombohedral structure is satisfactory. The same structure can also be used to provide an alternative indexation of the external set of reflections with sixfold symmetry to $30\bar{3}$ reflections from grains containing a rhombohedral unit cell (Table 1). According to this analysis, $\{\bar{1}\bar{1}2\}$ and $\{30\bar{3}\}$ planes have their normal oriented parallel to the shear plane, i.e. the [111] direction of the rhombohedral unit cell is perpendicular to the shear plane. The distorted rhombohedral structure corresponds to a cubic unit cell that has been "stretched" along a [111] direction such that all three angles are changed from 90° to about 115° (Table 2) and the cell parameter is increased. The [111] direction is significant because in the sheared fcc/hcp structure it is coincident with the shear-gradient direction. It is thus suggested that a rhombohedral structure originates in the gradient of shear stress across the gap of the Couette cell, which leads to effective normal stresses that break the cubic lattice symmetry. It has to be emphasized that the rhombohedral structure is observed under quiescent conditions, suggesting that it may be a metastable or at a least relatively long lived transient phase rather than a purely shear-induced structure. Further work will be required to elucidate the relaxation process following shear before definite conclusions can be drawn.

Turning to the determination of the space group of the rhombohedral unit cell, Miller indices that result from the indexation assuming a rhombohedral unit cell (Table 1) correspond to any one of the space groups of the rhombohedral system, for which there are no special reflection conditions [15]. Noting that

Table 2 Unit cell parameters. The cell parameters of the face-centred cubic and rhombohedral lattices were calculated according to the indexation in Table 1

Temperature (°C)	$\dot{\gamma}$ (s^{-1})	a_{fcc} (Å)[a]	10^7 V_{fcc} ($Å^3$)[b]	a_r (Å)[c]	α_r (degrees)[d]	10^7 V_r ($Å^3$)[e]
20	20	258.7	1.7	301.3	114.6	1.6
20	0	258.8	1.7	301.0	114.6	1.6
50	400	256	1.7	–	–	–
50	0	260.5	1.8	298.2	114.3	1.6

[a] Cell parameter of the face-centred cubic lattice
[b] Volume of the face-centred cubic unit cell
[c] Cell parameter of the rhombohedral lattice
[d] Angle of the rhombohedral lattice
[e] Volume of the rhombohedral unit cell

$q^* = (0.0420 \pm 0.0007)$ Å^{-1} for the as-mounted sample, Table 1 shows that this value was not significantly reduced under shear flow, and therefore fcc grains are expected to retain a close-packed structure under application and cessation of shear. Therefore, in keeping with the notion that within the fcc domains the micelles are arranged with the greatest possible density, the most satisfactory space group for the rhombohedral unit cell is likely to be that which satisfies the same. Suitable space groups are $R\bar{3}m$, $R3m$ or $P\bar{3}m1$ since they contain the space subgroup $Pm31$ that is the minimal group of symmetry common to all close-packed arrangements [18]. $Pm31$ includes the point group $3m$, which corresponds to the symmetry of a pair of closest-packed layers (each with symmetry $6m$) arranged in an AB... stacking sequence [18].

Although we cannot assign an unambiguous space group at the present time, we tentatively identify the space group as $R\bar{3}m$ for the following reasons. First, to our knowledge, $R3m$ or $P\bar{3}m1$ have never been identified as space groups of any surfactant system. Second, of the three space groups, two are centrosymmetric ($R\bar{3}m$ and $P\bar{3}m1$) while the third ($R3m$) is not [15]. Within the centrosymmetric groups, $R\bar{3}m$ has the highest symmetry [15], and is favoured for this reason. Third, $R\bar{3}m$ has been assigned to the rhombohedral phase in several lyotropic systems, including aqueous solutions of egg lecithin, divalent cationic soaps and nonaethylene glycol mono(11-oxa-14,18,22,26-tetramethylheptacosyl)ether [19]. These correspond to bicontinuous phases where the structural objects are represented by rods. They are linked three-by-three to form planar two-dimensional hexagonal networks regularly stacked in ABC... or AB... sequences, in a three-dimensional rhombohedral lattice [19]. In diblock copolymer melts, the hexagonally perforated layer structure of poly(styrene)–poly(isoprene) diblock copolymers has been ascribed to space group $R\bar{3}m$, which has been described as an ABC... stacking of hexagonal perforated sheets [20]. Therefore, assuming a $R\bar{3}m$ space group, the rhombohedral grains of $S_{13}E_{60}$ will certainly contain unit cells with a stacking of close-packed planes in ABC... or AB... sequences [19, 20]. This is qualitatively consistent with the previously discussed stacking of close-packed layers within fcc grains and favours the general picture of the three-dimensional rhombohedral phase as a deformation of the cubic phase [21]. This is supported by the observation that the set of $30\bar{3}$ reflections can be indexed to either a rhombohedral or a fcc unit cell (Table 1).

In conclusion, the diffraction patterns shown in Fig. 2a and b can be understood as a superposition of the three schematic patterns shown in Fig. 3. In keeping with the particular mixture of ABC... and AB... layer stacking for fcc grains, Bragg spots on the external and internal rings with sixfold symmetry in Fig. 2a and b have been arbitrarily indexed in Fig. 3b using the Miller indices of a three-dimensional hexagonal cell, with the [001] direction of the three-dimensional hexagonal cell perpendicular to the ($\mathbf{q_v}$, $\mathbf{q_e}$) plane.

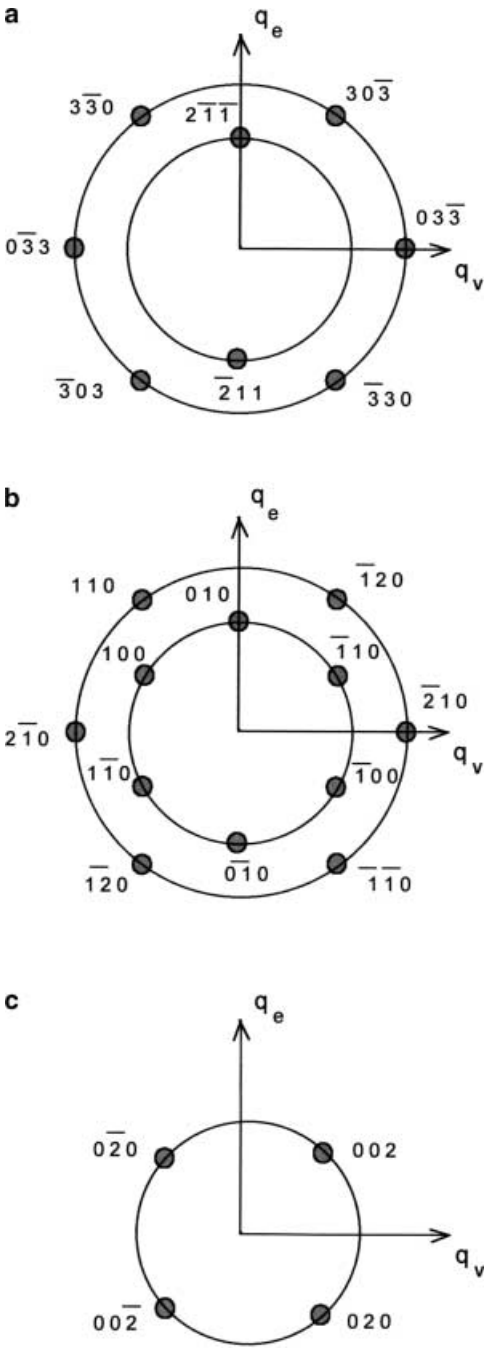

Fig. 3 Indexing of SAXS patterns in the ($\mathbf{q_v}$, $\mathbf{q_e}$) plane obtained from **a** a rhombohedral lattice oriented with a [111] direction perpendicular to the shear plane, **b** hexagonal close-packed lattice oriented with a [001] direction perpendicular to the shear plane, **c** two set of grains with face-centred cubic symmetry oriented with [110] direction parallel to $\mathbf{q_v}$. The diffraction patterns in Fig. 2a, b and d correspond to a superposition of **a**, **b** and **c**. The diffraction pattern in Fig. 2c corresponds to a superposition of **b** and **c**

The indexation shown in Fig. 3 can also be applied to the diffraction patterns previously obtained for aqueous gels of $E_{55}B_8$ [5] and $E_{40}B_{10}$ [6] subjected to steady shear. For these systems, a splitting in the meridional direction of the first-order reflection for the as-mounted sample was also observed under shear flow, although the average position between both scattering peaks was used to index the diffraction patterns.

The coexistence of two different structural organizations under shear flow was also investigated at 20 °C by rheology experiments. The stress versus shear rate, for $0.01 \leq \dot{\gamma}/s^{-1} \leq 800$, is shown in Fig. 4. The flow curve shows a range, $0.1 \leq \dot{\gamma}/s^{-1} \leq 40$, over which the stress almost saturates in a plateau at about 360 Pa. Within this plateau it is expected that fcc and rhombohedral structures coexist in the system, each having a different associated viscocity, while shear rates higher and lower than this interval should correspond to pure fcc or rhombohedral lattices, respectively; however, additional experiments would be necessary to pinpoint the location of the distorted grains.

Our SAXS experiments show that fcc and rhombohedral grains coexist under shear flow for shear rates in the range $20 \leq \dot{\gamma}/s^{-1} \leq 200$, even though this interval is larger than the plateau range observed in the flow curve (Fig. 4). This indicates that the section of the flow curve in which $\dot{\gamma}$ increases from 40 to 200 s^{-1} and the shear stress increases by 14% does not correspond to a state of pure orientation but to a regime in which the orientation attained by the crystal structure present in the system increases. We note here that gradients in the shear field cannot account for this observation because such gradients are only of the order of a few percent. This is in contrast to previous work [10], where the shear gradient was larger owing to a smaller Couette cell radius and larger gap than used here.

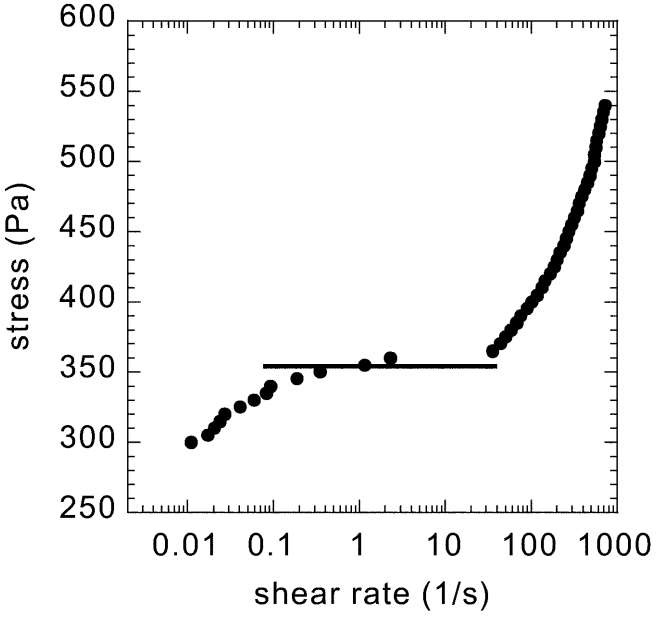

Fig. 4 Shear stress as a function of the shear rate for 30wt% $S_{13}E_{60}$ sample at 20 °C. The *line* is a guide to the eye

Upon increasing the temperature to 50 °C and the shear rate to $\dot{\gamma} = 400\ s^{-1}$, some changes in the diffraction pattern can be observed by comparing Fig. 2c to Fig. 2a and b. First of all, the broadening of $\bar{1}\bar{1}2$ reflections in the direction of $\mathbf{q}_v$ leads to a fusion of the meridional 111 and $\bar{1}\bar{1}2$ reflections (Fig. 2c) and the pattern resembles that for hcp/fcc grains only, which can be modelled by the superposition of diagrams shown in Fig. 2b and c. However, it is possible that the presence of rhombohedral grains is obscured by the strong flow imposed on the sample at such a high shear rate, which leads to a "smearing out" of the diffraction pattern. Indeed the SAXS pattern obtained at rest (Fig. 2d) clearly confirms the presence of a proportion of such grains owing to the presence of well-defined meridional $\bar{1}\bar{1}2$ reflections. The diffraction pattern can then be indexed according to the superposition of the diagrams shown in Fig. 3 and already discussed in the context of Fig. 2a and b. The data shown in Fig. 2 also clearly show that the highest degree of alignment of the crystal grains is attained under quiescent conditions following shear at a high shear rate.

It is noteworthy that q^* was not significantly reduced under shear flow (Table 1), although this is expected in the sliding-layer regime of flowing hcp layers which leads to SAXS patterns of the type shown in Fig. 2 [5, 8]. The partial orientation of the as-mounted sample might have lead to a reduction in q^* prior to shearing. Because it did not vary under the shear conditions employed, it is possible to use q^* for the as-mounted sample to estimate the micellar mass in the gel. The calculations assume a density of anhydrous copolymer $\rho_a \approx 1.13\ gcm^{-3}$, previously reported from the densities of the component polymers [12], which leads to a gel density $\rho_g \approx 3.39 \times 10^{-25}\ gcm^{-3}$ for a 30 wt% solution of $S_{13}E_{60}$ in water. The mass per unit cell (volume $a^3 = 258.9^3\ Å^3 = 1.7 \times 10^7\ Å^3$) is 5.84×10^{-18} g, hence the mass per micelle is 1.46×10^{-18} g (assuming four micelles per unit cell corresponding to a fcc structure), i.e. the micellar molar mass in the gel is $8.8 \times 10^5\ gmol^{-1}$ and $N_w = 206$ (calculated from $M_n = 4290\ gmol^{-1}$). The micellar molar mass determined for the dilute solution ($4.5 \times 10^5\ gmol^{-1}$) [12] together with $N_w = 102$ [12] show the same increase of micellar mass and association number on passing from micellar solution to gel under shear flow which has been previously noted for $E_{86}B_{10}$ solutions in 0.2 M K_2SO_4 [7]. Although the effect for $E_{86}B_{10}$ was much larger than determined here, it was ascribed to the dynamic equilibrium between micelles and molecules, which leads to a growth of the micelles in the gel in order to attain the correct packing condition. One interpretation of the SAXS data that would bring

the micelle molar mass in the gel into agreement with the dilute solution value would be to assume that there are eight micelles per unit cell instead of four as in the simplest $Fm\bar{3}m$ structure.

The calculation in the preceding paragraph referred to fcc grains at rest, but it can be extended to rhombohedral and fcc cells for the system under shear flow because they have roughly the same volume as fcc cells for the as-mounted sample. This is confirmed by the calculated cell parameters listed in Table 2, which correspond to an average copolymer mass per unit cell of 5.7×10^{-18} g, leading to an average micellar molar mass in the gel of 8.6×10^5 gmol^{-1} and $N_w = 200$. In particular, since fcc cells and rhombohedral cells have nearly the same volume, it seems likely that there are four micelles per rhombohedral unit cell as well as per fcc unit cell. The number of micelles per rhombohedral unit cell could increase to eight, in keeping with the notion mentioned in the previous paragraph to bring the micelle molar mass and N_w in the gel into agreement with the dilute solution, i.e. by assuming eight micelles per fcc unit cell. This result shows that the structure of rhombohedral grains is more complex than a primitive cell (containing one micelle per unit cell). The low number of indexed reflections does not allow a calculation of the electronic density map, which could give information about the position of the micelles in the unit cell. However, a structure containing up to eight micelles per unit cell is allowed within the $R\bar{3}m$ space group, since the number of special positions is enough to allocate eight micelles [15].

In this report we have established that shear rates in the range $20 \leq \dot{\gamma}/s^{-1} \leq 200$ lead to a fraction of rhombohedral grains, as well as the predominant fcc structure, in an aqueous solution of diblock $S_{13}E_{60}$. When the temperature is increased to 50 °C and the shear rate to 400 s^{-1}, the structure in the system mainly comprises fcc grains; however, upon cessation of shear a highly oriented pattern corresponding to coexisting fcc and rhombohedral grains is obtained.

Acknowledgements V.C. and P.H. were supported by the EU-TMR network "Complex architectures in diblock copolymer based polymer systems". Beamtime at Daresbury was provided under grant GR/M51994 from the Engineering and Physical Sciences Research Council (UK) to I.W.H. V.C. thanks G. Punte for helpful discussions.

References

1. Hamley IW (2001) Phil Trans R Soc Lond (in press)
2. Hamley IW (2000) Curr Opin Colloid Interface Sci 5:342
3. Mortensen K (1998) Curr Opin Colloid Interface Sci 3:12
4. Butler PD (1999) Curr Opin Colloid Interface Sci 4:214
5. Daniel C, Hamley IW, Mingvanish W, Booth C (2000) Macromolecules 33:2163
6. (a) Hamley IW, Pople JA, Fairclough JPA, Terrill NJ, Ryan AJ, Booth C, Yu GE, Diat O, Almdal K, Mortensen K, Vigild M (1998) J Chem Phys 108:6929; (b) Hamley I, Pople JA, Diat O (1998) Colloid Polym Sci 276:446
7. Hamley IW, Pople JA, Booth C, Derici L, Impéror-Clerc M, Davidson P (1998) Phys Rev E 58:7620
8. (a) McConnell GA, Lin MY, Gast AP (1995) Macromolecules 28:6754; (b) Ackerson BJ (1990) J Rheol 34:553; (c) Loose W, Ackerson BJ (1994) J Chem Phys 101:7211
9. Rehage M, H.Hoffmann H (1991) Mol Phys 74:933
10. Eiser E, Molino F, Porte G, Diat O (2000) Phys Rev E 61:6759
11. Eiser E, Molino F, Porte G (2000) Euro Phys J E 2:39
12. Kelarakis A, Rekatas C, Mai SM, Havredaki V, Ryan AJ, Hamley IW, Martini LGA, Attwood D, Booth C (2000) Macromol Chem Phys (in press)
13. Towns-Andrews E, Berry A, Bordas J, Mant GR, Murray PK, Roberts K, Sumner I, Worgan JS, Lewis E, Gabriel A (1989) Rev Sci Instrum 60:2346
14. Pople JA, Hamley IW, Diakun GP (1998) Rev Sci Instrum 69:3015
15. (1959) International tables for X-ray crystallography, vol II. Kynoch, Birmingham
16. Molino FR, Berret JF, Porte G, Diat O, Lindner P (1998) Eur Phys J B 3:59
17. Phoon CL, Higgins JS, Allegra G, van Leeuwen P, Staples E (1993) Proc R Soc Lond Ser A 442:221
18. Giacovazzo C, Monaco HL, Viterbo D, Scordari F, Gilli G, Zanotti G, Catti M (1992) Fundamentals of crystallography. Oxford University Press, New York
19. (a) Luzzati V, Gulik-Krzywicki T, Tardieu A (1968) Nature 218:1031; (b) Luzzati V, Tardieu A, Gulik-Krzywicki T (1968) Nature 217:1028; (c) Fairhurst CE, Holmes MC, Leaver MS (1996) Langmuir 12:6336
20. Förster S, Khandpur AK, Zhao J, Bates FS, Hamley IW, Ryan AJ, Bras W (1994) Macromolecules 27: 6922
21. Kékicheff P, Cabane B (1987) J Phys Paris 48:1571